J Mol Model
DOI 10.1007/s00894-012-1672-0

ORIGINAL PAPER

Interaction between shrimp and white spot syndrome virus through PmRab7-VP28 complex: an insight using simulation and docking studies

Arunima Kumar Verma · Shipra Gupta · Sharad Verma · Abha Mishra · N. S. Nagpure · Shivesh Pratap Singh · Ajey Kumar Pathak · Uttam Kumar Sarkar · Shri Prakash Singh · Mahender Singh · Prahlad Kishore Seth

Received: 5 September 2012 / Accepted: 29 October 2012

Abstract White spot disease is a devastating disease of shrimp *Penaeus monodon* in which the shrimp receptor protein PmRab7 interacts with viral envelop protein VP28 to form PmRab7–VP28 complex, which causes initiation of the disease. The molecular mechanism implicated in the disease, the dynamic behavior of proteins as well as interaction between both the biological counterparts that crafts a micro-environment feasible for entry of virus into the shrimp is still unknown. In the present study, we applied molecular modeling (MM), molecular dynamics (MD) and docking to compute surface mapping of infective amino acid residues between interacting proteins. Our result showed that α-helix of PmRab7 (encompassing Ser74, Ile143, Thr184, Arg53, Asn144, Thr184, Arg53, Arg79) interacts with β-sheets of VP28 (containing Ser74, Ile143, Thr184, Arg53, Asn144, Thr184, Arg53, Arg79) and Arg69-Ser74, Val75-Ile143, Leu73-Ile143, Arg79-Asn144, Ala198-Ala182 bonds contributed in the formation of PmRab7–VP28 complex. Further studies on the amino acid residues and bonds may open new possibilities for preventing PmRab7–VP28 complex formation, thus reducing chances of WSD. The quantitative predictions provide a scope for experimental testing in future as well as endow with a straightforward evidence to comprehend cellular mechanisms underlying the disease.

Keywords Docking · Molecular dynamics · Molecular modeling · Shrimp · Simulation · White spot disease

A. K. Verma · N. S. Nagpure (✉) · A. K. Pathak · U. K. Sarkar · S. P. Singh · M. Singh
Molecular Biology and Biotechnology Division, National Bureau of Fish Genetic Resources, Indian Council of Agricultural Research, Canal Ring Road, P.O. Dilkusha, Lucknow 226002 Uttar Pradesh, India
e-mail: nagpurens@yahoo.co.in

N. S. Nagpure
e-mail: nsnagpure@gmail.com

S. Gupta · P. K. Seth
Bioinformatics Centre, Biotech Park, Sector-G, Jankipuram, Lucknow 226021 Uttar Pradesh, India

S. P. Singh
Department of Zoology, Autonomous Government P.G. College, Satna, Madhya Pradesh, India

S. Verma · A. Mishra
School of Biochemical Engineering, Indian Institute of Technology, Banaras Hindu University, Varanasi, Uttar Pradesh, India

S. Gupta
Amity Institute of Biotechnology, Amity University Haryana, Amity Education Valley, Manesar, Gurgaon 122 413 Haryana, India

Introduction

Protein–protein interactions orchestrate plentiful biological processes involved during enigmatic cascading of the pathogen ingression into host to cause a fatal disease. White spot disease (WSD) caused by white spot syndrome virus (WSSV) is one serious disease that has drastically reduced the shrimp aquaculture production during the past two decades. WSD appeared for the first time in 1992 when WSSV caused a devastating blow to the population of shrimp *Penaeus monodon* and even spread to all of Southeast Asia

Published online: 23 November 2012

within a decade [1]. The deadliest form of WSSV caused upto 100 % shrimp mortality within 3–10 days [2]. Thus, development of proficient disease-free broodstock and effectual treatment of shrimp viruses to augment shrimp aquaculture and production became a global apprehension. Though employment of conducive wet lab methodologies have served as an indispensable tool for comprehensive understanding of disease mechanism [3], the availability of bioinformatics tools and methodologies such as molecular dynamics and docking [4–6] have elevated the understanding of host-parasite interaction at the atomic level. The structures of host and pathogen proteins generated by high-throughput X-ray crystallography and NMR spectroscopy have transformed the opportunities to use protein three-dimensional structures to accelerate drug discovery [7]. In addition, a radical leap in the field of drug discovery occurred by use of the 3D models of proteins generated from comparative/homology modeling. In this view, our study focuses on an *insilico* approach applying molecular modeling, dynamics and docking for understanding the interplay between the host-pathogen proteins through computational surface mapping of infective amino acid residues.

Complete genome sequencing of WSSV [8] ensured characterization of its genome at molecular level and elevated the understanding of WSD by protein-protein interaction between shrimp and virus [9]. As per the proposed model of morphogenesis of WSSV [1] when the virus enters host, the viral envelop proteins interact with endosomal proteins of shrimp, thereafter the naked viral nucleocapsid is transported into the shrimp nucleus where viral genome is released for its replication and dissemination. In this line, many reports are available that show that the pathogens intrude into host by endocytosis [10] and hijack the Rab-mediated trafficking machineries [11] to endure inside the host endosome. Therefore, targeting the Rab proteins might devise remedial measures against diseases [12]. The shrimp protein PmRab7 is a Rab protein located in endosome [13] and acts as receptor for the WSSV envelop protein VP28 [14]. VP28 is a major structural envelope protein of WSSV largely accountable for the systemic infection in shrimp [14]. It also forms an important part of "infectome" crucial in cell recognition, attaching and guiding the virus into the shrimp cell [15]. Crystal structure studies conducted on VP28 revealed that it is located on the outer surface of the virus and composed of C–terminal nine stranded β–barrel and N–terminal α–helix [16].

In order to investigate the mechanism of interaction between shrimp and virus proteins, we designed 3D structure of shrimp receptor protein PmRab7 and downloaded the available structure of VP28 from Protein Data Bank (PDB_ID: 2ED6). After initial energy validation of both structures, they were simulated for understanding behavior of both proteins individually. Further energy of simulated proteins was checked by various validation servers to ensure that the proteins are stable enough to serve as optimized inputs for docking. The docked complex obtained served as an initial complex configuration/conformation onto which further simulation was performed to get insight into detailed dynamics of PmRab7-VP28 complex. The study was performed with a motive to find infective surface amino acid residues as well as bonds involved in complex formation that may serve as targets for further drug development work. Disruption of such bonds or alteration in infective amino acid residues can help in blocking at least one route of entry of virus into the shrimp that may in turn reduce the spread of WSD. The outcome of this study provides (i) amino acid site recognition of the PmRab7 protein that come in direct contact with virus protein; (ii) the mechanism of initial entry of virus into the shrimp; (iii) the host–parasite interaction involved in WSSV infection. The structural studies of VP28 and PmRab7 can provide molecular targets for the development of therapeutic strategies based on the blockage of target cell binding.

Methods

Cross species analysis, selection of template and preparation of macromolecule

The cross species analysis of Rab7 protein across ten vertebrates (Table 1) was performed by ClustalW, a multiple sequence alignment (MSA) tool using default parameters to detect conserved regions on Rab7 and search suitable template for predicting the 3D structure of PmRab7. The suitable template was later confirmed by ModWeb server [17] and by performing protein BLAST [18] using PDB database [19]. The 3D structure of PmRab7 was designed using RatRab7 (PDB_ID: 1VG8) as a template [20] by Modeller9v8 [21]. Loop, side chain modeling and energy minimization were done using Swiss PDB Viewer software (http://spdbv.vital-it.ch/).

Model validation and structural characterization

Structural Analysis and Verification Server (SAVES) (http://nihserver.mbi.ucla.edu/SAVES/) was used to ensure the quality of the generated 3D structure of proteins PmRab7 and VP28. Evaluation and validation of the protein structures were done with PROCHECK [22], ERRAT [23], WHAT-IF [24], ProSA[25], VERIFY3D [26]. Chimera [27], PyMolv0.99 (http://www.pymol.org) and Discovery Studio Visualizer2.5 (http://accelrys.com) softwares were used for visualizing the 3D structure of proteins. Detailed insight into the secondary structure arrangement of PmRab7 and VP28 was carried out using CATH database [28].

Table 1 GenBank accession numbers of Rab7 proteins across ten vertebrate species

Organisms	Accession no.	Organisms	Accession no.
Mouse	CAA61797	Zebrafish	AAH54602
Rat	BAE17000	Common carp	ACK77787
Human	AAD02565	Sea anemone	JC8006
Dog	NP_001003316	Giant tiger shrimp	ABB70064
Rabbit	AAD02564	Pacific white shrimp	ACT65737

Molecular dynamics simulations of PmRab7 and VP28

Molecular dynamics simulations of PmRab7 and VP28 were performed using the GROMACS 4.5.3 [29] (http://www.gromacs.org/) under OPLS 2005 atoms force field on Pentium (R) dual-core processor machine. The 3D structure of PmRab7 was immersed in a cubic box of 0.85 nm and periodic boundary conditions were applied using editconf tool followed by addition of 21,668 SPC water molecules. System was made electrically neutral by adding 2 Na^+ using the 'genion' tool. The system was first minimized for energy in 1000 steps by steepest descent method to remove excessive strain. The minimized system was then subjected to MD in two steps. Initially NVT ensemble (constant number of particles, volume, and temperature) was performed for 500 ps, followed NPT ensemble (constant number of particles, pressure, and temperature) for 500 ps. The well equilibrated system was then subjected to molecular dynamics simulations for 9 ns. The total number of atoms in system was 72,691. Temperature was kept constant at 300 K with Andersen thermostat, pressure coupling of 1 bar with Berendsen algorithm and system was further allowed to undergo production runs. LINCS algorithm [30] was used to constrain the lengths of all bonds while the waters molecules were restrained using the SETTLE algorithm [31]. The trajectory files were analyzed by using g_rms and g_gyrate utilities of GROMACS to obtain the root-mean-square deviation (RMSD) and radius of gyration (Rg) values. RMSD values for Cα atoms from the initial structure were considered as a necessary condition to determine the convergence of the proteins toward equilibrium and calculated by:

$$RMSD(t_1, t_2) = \left[\frac{1}{M}\sum_{i=1}^{N} m_i \left\| r_i(t_1) - r_i(t_2) \right\|^2\right]^{\frac{1}{2}},$$

where $\sum_{i=1}^{N} m_i$ and $r_i(t)$ is the position of atom i at time t. The shape of protein molecule at all instants of simulation is indicated through hydrodynamic radius obtained using radius of gyration calculated by: $R_g = \left(\frac{\sum_i \|r_i\|^2 m_i}{\sum_i m_i}\right)^{\frac{1}{2}} m_i$ is mass of atom i and r_i position of atom i with respect to the center of mass of the molecule. The same approach was used to simulate VP28 under the similar conditions (300 K temperature and 1 bar pressure) for 9 ns. Eight Na^+ and 19,256 SPC water molecules were used during simulation of VP28 and a total of 60,323 atoms were present in the system. The simulated 3D model of PmRab7 was submitted to Protein Model DataBase (http://mi.caspur.it/PMDB/).

Localization of VP28 across the viral envelop

MSA using Multalign [32] followed by transmembrane prediction program SOSUI [33] were employed to reveal the structural complexities and understand the location of VP28. Uncrystallized VP28 (UniProt_ID: Q9ICB7) and various chains of crystallized VP28 protein (PDB_ID: 2ED6) were considered as input.

Molecular docking

Protein docking between PmRab7 and VP28 was done using PatchDock server (http://bioinfo3d.cs.tau.ac.il/PatchDock/) [34] with default settings. PatchDock server is widely used for the protein−protein docking studies [35–37] and the algorithm carries out rigid docking with surface flexibility addressed by intermolecular penetration.

Molecular dynamics simulation of PmRab7-VP28 complex

Molecular dynamics simulations of PmRab7-VP28 complex was performed using the GROMACS 4.5.3 under gromos43a1 force field [29]. The whole simulation experiment was done for 13 ns by using 26,553 SPC water molecules and 10 Na^+ ions. The same methodology was adopted for simulation of this complex as done in the MD of individual proteins PmRab7 and VP28. The trajectory files were analyzed by using g_rms and g_gyrate utilities of GROMACS to obtain the RMSD and Rg values while van der Waals and short range electrostatic energies were computed in order to obtain information about the stability of the complex [38, 39]. Snapshots of the docked complex were generated by PyMolv0.99 and Discovery Studio Visualizer 2.5 software in order to visualize the pictorial depiction of the interaction between both proteins.

Fig. 1 Cross species analysis of Rab7 protein

Results

Molecular modeling, quality assessment and structural characterization

MSA across ten species of Rab7 proteins depicted the presence of conserved regions (Fig. 1) as well as predicted RatRab7 as a suitable template for modeling structure of PmRab7. RatRab7 was further confirmed as one of the suitable template for modeling 3D structure of PmRab7 from BLAST and ModWeb server. Five models were generated out of which the model that showed the least RMSD with respect to the crystal structure of the template, optimal discrete optimized potential energy (DOPE) and GA314 score was selected for refinement. Table 2 presents the summarized results obtained from various servers. Our analysis showed that 94.7 % and 91.2 % residues of PmRab7 and VP28 were in the most favorable region, 5.3 % and 8.2 % residues were in allowed region respectively and none in the disallowed region. RMSD between the Cα atom of the template RatRab7 and PmRab7 was 0.207 Å, which indicated high structural homology between model and template (Fig. 2). The G factor (−0.2), Prosa, Errat and Verify3D of the PmRab7 fit well within the array of a high quality model. The CATH prediction for PmRab7 depicted a characteristic Rossmann fold having α-β-α sandwich like architecture involved in GTPase activity while for VP28 showed to contain mainly beta sheets and belongs to immunoglobulin super family.

Molecular dynamics and energy validation of PmRab7 and VP28

The RMSD trajectories showed that PmRab7 and VP28 became stable at 7.7 ns and 6.0 ns respectively (Fig. 3). RMSD values for PmRab7 increased from 0.99 nm to 1.044 nm at 2.4 ns followed by atomic fluctuation within protein that leveled off around 7.7 ns (0.51 nm) and then demonstrated a stable trajectory between 0.49 nm and 0.51 nm. The RMSD value for VP28 starts from 0.001 nm and increases to 0.19 nm around 1.3 ns followed by sharp increase of 0.26 nm at 4.8 ns and decrease to 0.13 nm at 5.6 ns and finally becomes stable after 6.0 ns between 0.17 nm–0.18 nm (Fig. 4). VP28 maintained its compactness during the entire simulation while PmRab7 faced minor changes, but overall compactness was maintained throughout simulation. Initially the Rg trajectory for PmRab7 was more compact showing dimension of 1.8 nm which steadily increased to 1.95 nm at 1.8 ns and elevated to 2.01 nm at 1.9 ns and finally attained stability after 6.3 ns between 2.0 nm and 2.2 nm (Fig. 5). Rg profile generated for VP28 is quite stable between 1.73 nm and 1.78 nm (Fig. 6). Table 2 lists the energy validation results of the simulated structures from various servers. At the end of simulation, we obtained

Table 2 Various scores obtained through different validation servers to depict the quality assessment of the different proteins used for the study

Validation servers/proteins	Procheck (in %)	Errat	G-Factor	Prosa	Verify_3D (in %)
PmRab7	94.7	87.302	0.02	−6.03	74.76
PmRab7[a]	94.7	87.302	0.02	−6.03	74.76
VP28	91.2	96.914	0.32	−6.49	82.46
VP28[a]	91.2	96.914	0.32	−6.49	82.46

[a] Shows the evaluation scores of protein after MD simulation from various servers

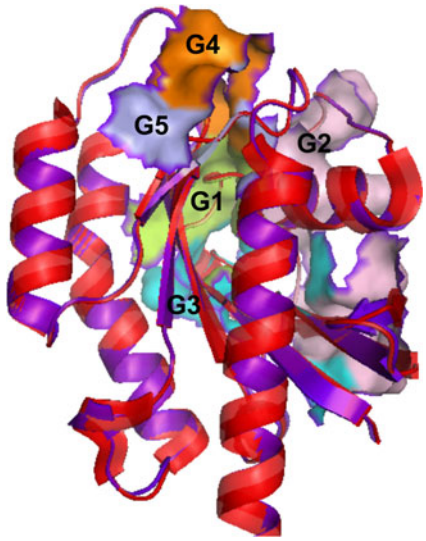

Fig. 2 3D structure superimposition of PmRab7 and RatRab7

the stable conformations of the proteins that served as optimized input for the docking algorithm. The simulated 3D structure of PmRab7 was submitted to Protein Model DataBase (PMDB_ID: PM0077992).

Transmembrane localization of VP28

Sequence alignment between crystallized VP28 (169 amino acid) and uncrystallized VP28 (204 amino acid) indicated a deficit of 32 amino acids toward N–terminal end and three amino acids toward C–terminal end in crystallized VP28. The crystal structure of VP28 started from the 32th postion of amino acid and ended at 201. The residues from 32 to 201 were 100 % identical in both the sequences. SOSUI prediction of crystallized VP28 gave a negative result for transmembrane prediction while uncrystallized VP28 revealed transmembrane region. The results altogether portrayed that N–terminal VP28 (amino acid 6–28) traverses the viral envelop while remaining protein (amino acid 28–204) hangs out of the viral envelope in order to interact with external biological moieties (Fig. 7).

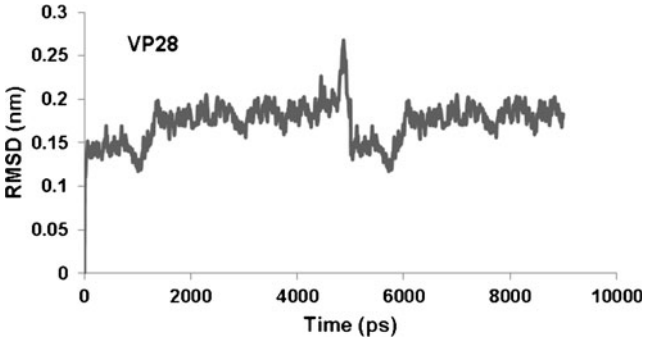

Fig. 4 RMSD graph of VP28

Docking of both proteins and molecular dynamics of the complex

Docking study between PmRab7 and VP28 revealed significant contribution of hydrogen bonds, attractive van der Waals, repulsive van der Waals, atomic contact energies and global interaction energy of −7.34, −51.27, 32.97, 13.96 and −31.91 ($kJmol^{-1}$) respectively. The complex is initially stabilized by nine hydrogen bonds. The PmRab7-VP28 complex with the binding energy −31.91 $kJmol^{-1}$ was further used for carrying out MD. RMSD for all backbone atoms, Rg, electrostatic energy, van der Waals energy of PmRab7−VP28 complex were studied in the form of MD trajectories. RMSD profiles always remained less than 0.6 nm for the entire simulation. The RMSD value for the PmRab7−VP28 complex increased from 0.059 nm to 0.41 nm at 4.1 ns, further constantly increased to attain 0.51 nm value at 10 ns and finally attained 0.52 nm around 11 ns depicting a constant RMSD profile during the simulation (Fig. 8). The constant trajectory depicted a stabilized complex formation which in turn depicted strong bonding between both the proteins. Rg of PmRab7-VP28 complex was analyzed to determine its compactness. Rg value of initial complex configuration is 2.25 nm followed by decrement in value to 2.14 nm around 7 ns. Thereafter the Rg

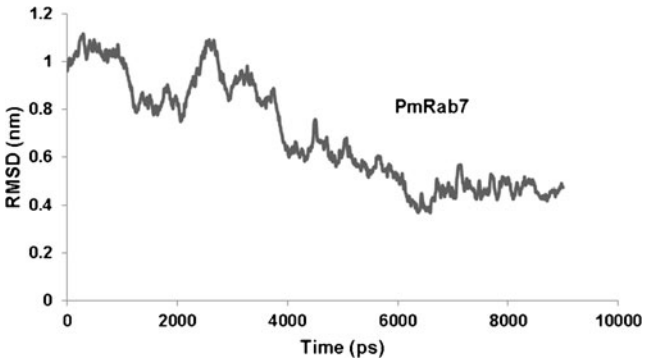

Fig. 3 RMSD graph of PmRab7

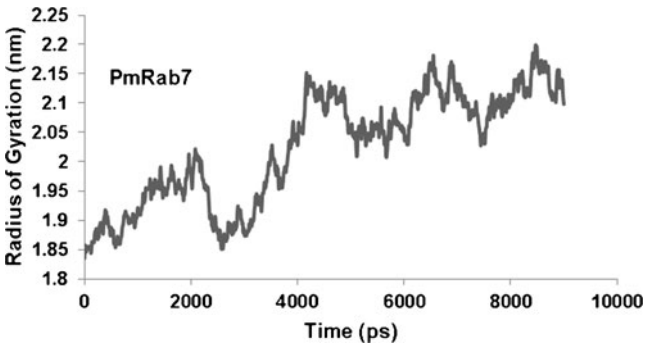

Fig. 5 Radius of gyration graph of PmRab7

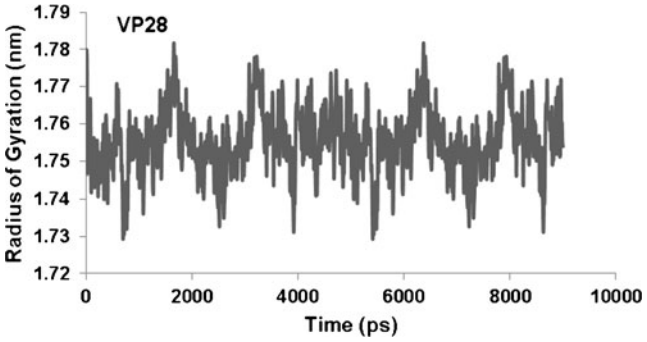

Fig. 6 Radius of gyration graph of VP28

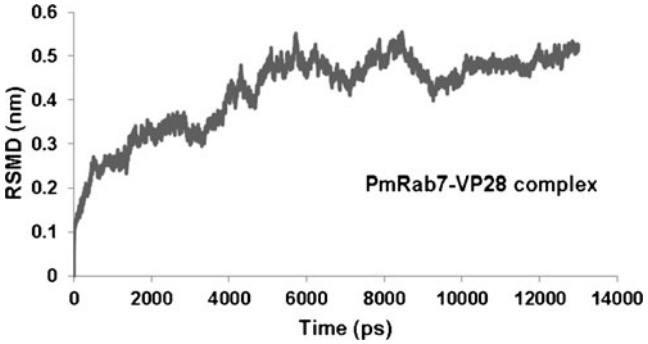

Fig. 8 RMSD graph of PmRab7-VP28 complex

further reduced to attain a constant value of 2.13 nm around 10 ns (Fig. 9). The trajectory shows that initial binding between both the proteins is loose but with progress in time the complex became more compact in turn suggesting the tight bonding between the shrimp and viral protein. To get a deeper insight into the stability as well as non-bonded energies of complex van der Waals energy was calculated that ranged from −459.2 to −5−77.49 kJmol^{-1} (Fig. 10). The trajectory for van der Waals energy is almost constant throughout the tenure of simulation. Short-range electrostatics of the complex was provided by electrostatic energy that ranged from −341.79129 to −648.61853 kJmol^{-1} (Fig. 11). Before the simulation of the complex 9H-bonds were traced between both the proteins, but with the start of simulation the number of H-bonds increased to 18 and π−π interactions could also be traced sandwiched within the complex. With increase in time the number of H-bonds increased to 33 at 4 ns. Furthermore, fluctuation in trends of H-bond and π−π formation was observed up to 7 ns where 30 H-bonds and 3 π−π interactions were observed. After 9 ns of simulation, a minor decrease in pattern of H-bond and π−π bond formation was seen. Thereafter, the number of H-bonds ranged between 16 and 18 and the π−π interactions were traced. The results altogether depicted that, the number of H-bonds and π−π interactions were almost similar at start and end of simulation, but the complex was found more stable at the end of simulation as suggested by stable RMSD and Rg values. In contrast, the RMSD and Rg graph in the beginning of simulation suggest that initially the complex was not stable. When H-bonds, π−π interaction, RMSD and Rg trajectory were considered around 7 ns, all four parameters suggested stability of the complex. The high value of H-bonds and π−π interaction also suggested that both counterpart proteins interacted closely with each other at this point of simulation. Figure 12 shows the snapshots of the simulated complex depicting the interaction between both

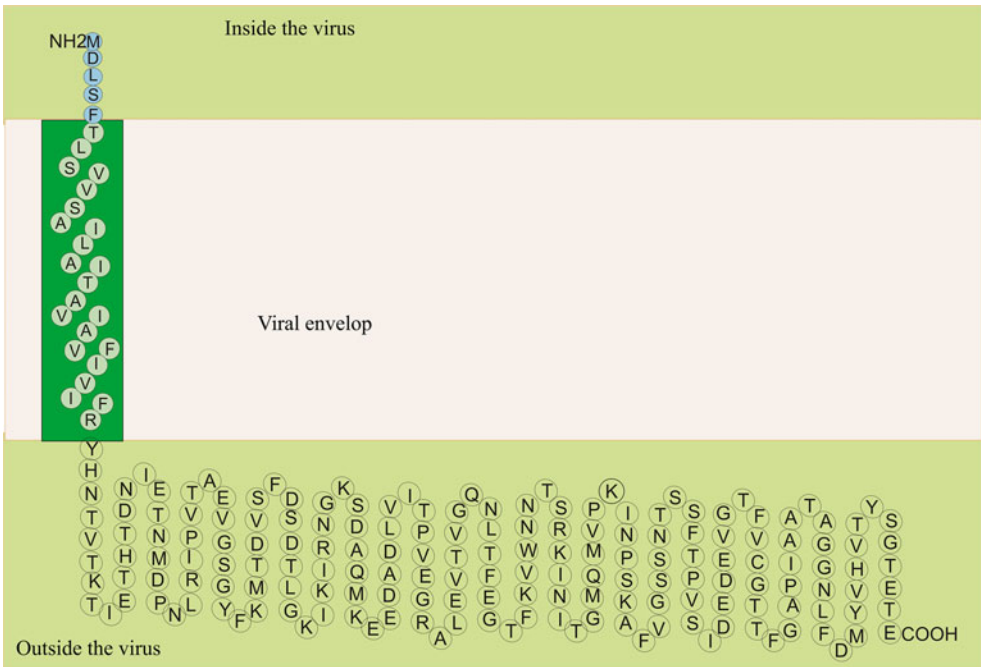

Fig. 7 Localization of VP28 within viral envelope showing α-helix of VP28 hanging out from viral envelop to anchor the C-terminal β-barrel of VP28 that further interacts with PmRab7 protein to induce systemic infection into the shrimp

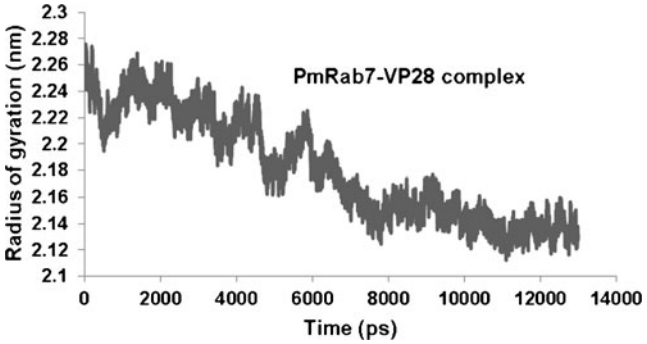

Fig. 9 Radius of gyration graph of PmRab7-VP28 complex

proteins. Furthermore, the receptive amino acid residues involved in the formation of complimentary surfaces are Arg69, Val75, Glu105, Leu73, Asp201, Arg79, Glu68 in PmRab7 and Ser74, Ile143, Thr184, Arg53, Asn144, Thr184, Arg53, Arg79 in VP28. In addition, the amino acid interactions that were prevalent for most of the tenure of simulation involved Arg69-Ser74, Val75-Ile143, Leu73-Ile143, Arg79-Asn144, Ala198-Ala182.

Discussion

The present study provides a suitable 3D model of PmRab7 that serves as an initial input for PmRab7-VP28 complex formation. The 3D model of PmRab7 when superimposed to the atomic coordinate sets of its template depicted optimal structural alignment and minimal RMSD (0.207 Å) suggests a strong homology between both proteins. The 3D model of PmRab7 was further checked for stereo-chemical parameters and overall structure geometry by various energy validation servers and found to fit well into the proficiency criteria of these servers, thus suggesting that the 3D structure generated is good both in terms of structure as well as energy parameters. CATH prediction for PmRab7 revealed presence of Rossmann fold having GTPase behavior and hence we presume that the protein might use GTP for helping virus entry in the host.

MD of PmRab7 and VP28 were done to understand individual behavior of PmRab7 and VP28 at atomic level. RMSD values for PmRab7 and VP28 suggested that though both proteins undergo fluctuations initially but at the end of tenure of simulation the trajectories become stable. Rg value for PmRab7 increases with time and stabilizes after 6 ns signifying that with increase in time the dimension of PmRab7 increases but the protein maintains its shape after 6 ns. Rg of VP28 remains almost stable throughout the simulation thus, suggesting that VP28 remains of same size throughout the simulation. The result from Procheck shows the residues in the allowed region of the Ramachandran plot and Errat depicts the statistics of non-bonded interactions between different atom types. VERIFY3D postulates the compatibility of the 3D atomic structure with its own amino acid sequence. The energy validations of the proteins ensure that both are energetically favorable and hence serve as an optimized input to the docking experiment. The structural complexity and localization of VP28 in the viral membrane was performed with the motive to get insight into domains of VP28 that interact with PmRab7. Prior studies revealed that the C–terminal domain of the VP28 protein was involved in receptor recognition whereas N–terminal portion remains embedded in the virus [13]. It has further been reported that the nine stranded β-barrel and one α-helix of VP28 were involved in systemic infection [13]. Our *insilico* findings indicated that N–terminal VP28 (amino acid 6–28) traverses the viral envelop while the remaining protein (amino acid 28–204 that consist of β-barrel) hangs out of the viral envelope. Infectivity resides in this β-barrel of VP28 while α-helix (toward N–terminus of VP28) acts as an anchorage to lodge VP28 firmly into the viral envelop. Thus, PmRab7 and β-barrel portion of VP28 were used for further docking procedures.

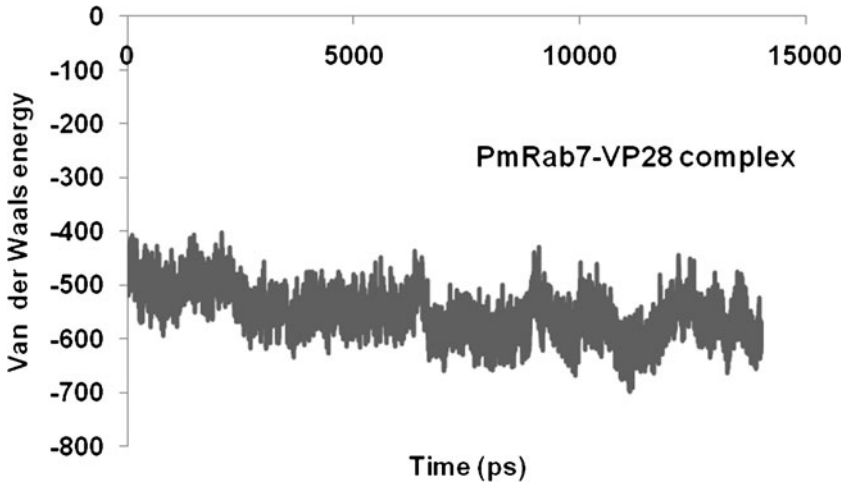

Fig. 10 Van der Waals energy graph of PmRab7-VP28 complex

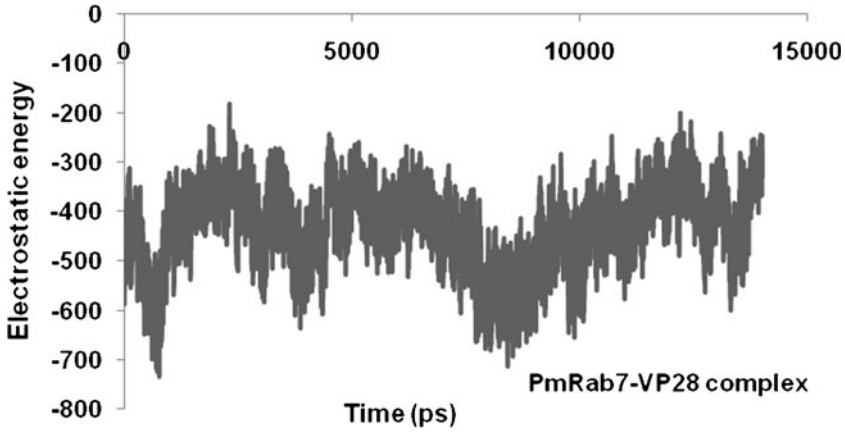

Fig. 11 Electrostatic energy graph of PmRab7-VP28 complex

Docking and MD tools have turned out an effective means for predicting the binding sites involved in protein–protein docking. The efficiency of docking algorithm has been validated by taking raw data from already published work and further running the same docking procedure. The concordant results have been obtained in both cases suggesting the competence of PatchDock as a good docking server [40]. The docking algorithm exploits the surface complementarities of residues present in the binding site based on how the scoring functions rank the various docking outputs [41–43]. The best docked conformation is judged on the basis of optimal geometric score, interface area size and desolvation energy generated by the complex. The *insilico* docking approaches based on surface geometry complementarities and amino acid pairwise affinities between PmRab7 and VP28 prefigure formation of hydrogen bond networks between amino acid residues lying in the interface of both proteins. We have also highlighted the new binding sites

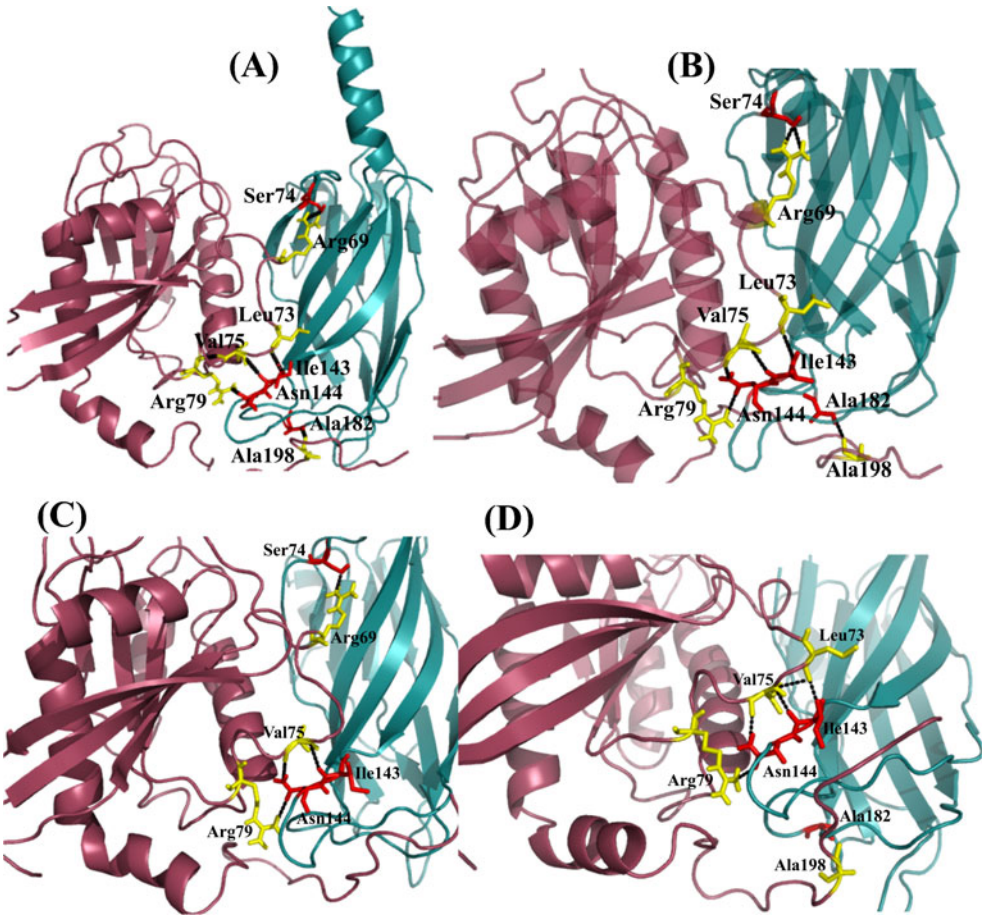

Fig. 12 Snapshots of molecular dynamics of PmRab7-VP28 complex during intervals (**a**) 3 ns (**b**) 7 ns (**c**) 11 ns (**d**) 13 ns. Protein-protein interaction are shown between viral envelop protein VP28 (*deepteal cyan*) and shrimp receptor protein in PmRab7 (*raspberry red*). Hydrogen bond between amino acids of PmRab7 and amino acids of VP28 are marked in *black color line*

using blind docking as well as utilizing different docking grids spanning various regions of the entire protein. The stable behavior of the PmRab7–VP28 complex is also attributed due to van der Waals forces and atomic contact energies. Van der Waals interaction energy is computed in order to derive a theoretical and quantitative evaluation of the protein–protein and non–bonded interactions. Prior to MD, the complex revealed presence of 9H-bonds between both the proteins. With initiation of simulation, π−π bonds could be located as well as the number of H-bonds increased to 18. Further increment of H-bonds to 33 at 4 ns indicated that with progress in simulation period the shrimp and viral proteins acclimatize each other in order to form a stable complex. Further fluctuations in trends of H-bond and π−π formation were observed at 7 ns (30H-bonds and 3 π−π interactions), at 11 ns (20H-bonds and 2 π−π interactions) and at 13 ns (18H-bonds and 1 π−π interactions). Thus after 9 ns of simulation a minor decrease in pattern of H-bond and π−π bond formation is observed suggesting that after a strong interaction for a trivial period the complex proteins show a very minor decrease in the bonding pattern. Rg results depict that with increase in simulation period the compactness of the complex increases suggesting more interaction till the complex stabilized. At 12–13 ns though the complex formed is stable enough the number of H-bonds and π−π bonds formed during the end of simulation decrease somewhat suggesting that both proteins try to depart (decrease mutual communication) from each other possibly in order to get involved in biological processes such as virus dissemination, propagation and duplication within the host [1]. The receptive amino acid residues involved in the formation of complimentary surfaces for both interacting proteins were Arg69, Val75, Glu105, Leu73, Asp201, Arg79 and Glu68 present on α-helix of PmRab7 and Ser74, Ile143, Thr184, Arg53, Asn144, Thr184, Arg53, Arg79 on β-sheets of VP28. These amino acid residues play a crucial role in interaction between host-parasite at molecular level and alteration of these residues can change the interacting complimentary surface thus de-stabilizing/prevent forming the PmRab7-VP28 complex. In addition to this, the amino acid interactions that were prevalent for most of the tenure of simulations involved Arg69-Ser74, Val75-Ile143, Leu73-Ile143, Arg79-Asn144, Ala198-Ala182. Disruption of such H-bonds that are present within the binding pocket of complex, can lead to prevention of PmRab7–VP28 complex formation.

Conclusions

We conclude, that when WSSV enters host, the envelop proteins of virus (VP28) fuse with endosomal host proteins (PmRab7) transiently after which the naked viral nucleocapsid is transported to the host nucleus where the viral genome replication starts. PmRab7 probably utilizes energy from GTP to help the virus enter into the host. During the transient contact between shrimp protein PmRab7 with the envelop protein VP28, a complex PmRab7−VP28 is formed. This complex has critical significance in WSD of shrimp as it is the starting point of shrimp and viral interaction and also elucidates intricate relationship between the host (shrimp) and pathogen (WSSV) at molecular level. In the complex, the α-helix of PmRab7 (encompassing Ser74, Ile143, Thr184, Arg53, Asn144, Thr184, Arg53, Arg79) interact with β-sheets of VP28 (containing Ser74, Ile143, Thr184, Arg53, Asn144, Thr184, Arg53, Arg79). Thus targeting these amino acid residues that form complimentary surfaces between PmRab7 and VP28 as well as disrupting Arg69-Ser74, Val75-Ile143, Leu73-Ile143, Arg79-Asn144, Ala198-Ala182 bonds can block at least one mode of virus entry into the shrimp. These conclusions may open new possibilities, challenges and opportunities for unfolding ventures into drug designing against WSSV. To our knowledge, this may be the first attempt toward understanding WSD by computational methodologies. This study may lead to a strong foundation for future experiments that can be used for controlling WSD.

Acknowledgments Authors are thankful to National Agricultural Bioinformatics Grid Project under National Agricultural Innovation Project, Indian Council of Agricultural Research, New Delhi for providing financial support. We also gratefully acknowledge the necessary facilities provided by the Director, National Bureau of Fish Genetic Resources, Lucknow and the Chief Executive Officer, Biotech Park, Lucknow.

References

1. Escobedo-Bonilla CM, Alday-Sanz V, Wille M, Sorgeloos P, Pensaert MB, Nauwynck HJ (2008) A review on the morphology, molecular characterization, morphogenesis and pathogenesis of white spot syndrome virus. J Fish Dis 31(1):1–18
2. Lightner DV (1996) Epizootiology, distribution and the impact on international trade of two penaeid shrimp viruses in the Americas. Rev Sci Tech 15(2):579–601
3. Huang HT, Leu JH, Huang PY, Chen LL (2012) A putative cell surface receptor for white spot syndrome virus is a member of a transporter superfamily. PLoS One 7(3):e33216
4. Kushwaha SK, Shakya M (2010) Protein interaction network analysis–approach for potential drug target identification in Mycobacterium tuberculosis. J Theor Biol 262(2):284–294
5. Awale M, Kumar V, Saravanan P, Mohan CG (2010) Homology modeling and atomic level binding study of Leishmania MAPK with inhibitors. J Mol Model 16(3):475–488
6. Gutiérrez-de-Terán H, Nervall M, Ersmark K, Liu P, Janka LK, Dunn B, Hallberg A, Aqvist J (2006) Inhibitor binding to the plasmepsin IV aspartic protease from *Plasmodium falciparum*. Biochemistry 45(35):10529–10541
7. Ode H, Nakashima M, Kitamura S, Sugiura W, Sato H (2012) Molecular dynamics simulation in virus research. Front Microbiol 3:258

8. Yang F, He J, Lin X, Li Q, Pan D, Zhang X, Xu X (2001) Complete genome sequence of the shrimp white spot bacilliform virus. J Virol 75(23):11811–11820
9. Lu L, Kwang J (2004) Identification of a novel shrimp protein phosphatase and its association with latency-related ORF427 of white spot syndrome virus. FEBS Lett 577(1–2):141–146
10. Sieczkarski SB, Whittaker GR (2002) Dissecting virus entry via endocytosis. J Gen Virol 83(Pt 7):1535–1545
11. Seabra MC, Mules EH, Hume AN (2002) Rab GTPases, intracellular traffic and disease. Trends Mol Med 8(1):23–30
12. Stein MP, Dong J, Wandinger-Ness A (2003) Rab proteins and endocytic trafficking: potential targets for therapeutic intervention. Adv Drug Deliv Rev 55(11):1421–1437
13. Sritunyalucksana K, Wannapapho W, Lo CF, Flegel TW (2006) PmRab7 is a VP28-binding protein involved in white spot syndrome virus infection in shrimp. J Virol 80(21):10734–10742
14. van Hulten MC, Witteveldt J, Snippe M, Vlak JM (2001) White spot syndrome virus envelope protein VP28 is involved in the systemic infection of shrimp. Virology 285(2):228–233
15. Chang YS, Liu WJ, Lee CC, Chou TL, Lee YT, Wu TS, Huang JY, Huang WT, Lee TL, Kou GH, Wang AH, Lo CF (2010) A 3D model of the membrane protein complex formed by the white spot syndrome virus structural proteins. PLoS One 5(5):e10718
16. Tang X, Wu J, Sivaraman J, Hew CL (2007) Crystal structures of major envelope proteins VP26 and VP28 from white spot syndrome virus shed light on their evolutionary relationship. J Virol 81(12):6709–6717
17. Eswar N, John B, Mirkovic N, Fiser A, Ilyin VA, Pieper U, Stuart AC, Marti-Renom MA, Madhusudhan MS, Yerkovich B, Sali A (2003) Tools for comparative protein structure modeling and analysis. Nucleic Acids Res 31(13):3375–3380
18. Altschul SF, Gish W, Miller W, Myers EW, Lipman DJ (1990) Basic local alignment search tool. J Mol Biol 215(3):403–410
19. Berman HM, Westbrook J, Feng Z, Gilliland G, Bhat TN, Weissig H, Shindyalov IN, Bourne PE (2000) The protein data bank. Nucleic Acids Res 28(1):235–242
20. Rak A, Pylypenko O, Niculae A, Pyatkov K, Goody RS, Alexandrov K (2004) Structure of the Rab7:REP-1 complex: insights into the mechanism of Rab prenylation and choroideremia disease. Cell 117(6):749–760
21. Sali A, Potterton L, Yuan F, Vlijmen H, Karplus M (1995) Evaluation of comparative protein modeling by MODELLER. Proteins 23(3):318–326
22. Laskowski RA, MacArthur MW, Moss DS, Thornton JM (1993) PROCHECK: a program to check the stereochemical quality of protein structures. J Appl Cryst 26:283–291
23. Colovos C, Yeates TO (1993) Verification of protein structures: patterns of nonbonded atomic interactions. Protein Sci 2(9):1511–1519
24. Vriend G (1990) WHAT IF: a molecular modeling and drug design program. J Mol Graph 8(1):52–56, 29
25. Wiederstein M, Sippl MJ (2007) ProSA-web: interactive web service for the recognition of errors in three-dimensional structures of proteins. Nucleic Acids Res 35:W407–W410
26. Bowie JU, Luthy R, Eisenberg D (1991) A method to identify protein sequences that fold into a known three-dimensional structure. Science 253(5016):164–170
27. Pettersen EF, Huang CC, Couch GS, Greenblatt DM, Meng EC, Ferrin TE (2004) UCSF Chimera–a visualization system for exploratory research and analysis. J Comput Chem 25(13):1605–1612
28. Orengo CA, Michie AD, Jones S, Jones DT, Swindells MB, Thornton JM (1997) CATH–a hierarchic classification of protein domain structures. Structure 5(8):1093–1108
29. Berendsen HJC, Van der Spoel D, Van Drunen R (1995) GROMACS—a message passing parallel molecular dynamics implementation. Phys Commun 91:43–56
30. Hess B, Bekker H, Berendsen HJC, Fraaije JGEM (1997) LINCS: a linear constraint solver for molecular simulations. J Comput Chem 16:273–284
31. Miyamoto S, Kollman PA (1992) SETTLE: an analytical version of the SHAKE and RATTLE algorithms for rigid water models. J Comput Chem 13:952–962
32. Corpet F (1988) Multiple sequence alignment with hierarchical clustering. Nucleic Acids Res 16(22):10881–10890
33. Hirokawa T, Boon-Chieng S, Mitaku S (1998) SOSUI: classification and secondary structure prediction system for membrane proteins. Bioinformatics 14(4):378–379
34. Schneidman-Duhovny D, Inbar Y, Nussinov R, Wolfson HJ (2005) PatchDock and SymmDock: servers for rigid and symmetric docking. Nucleic Acids Res 33:W363–W367
35. Sharma A, Nigam A (2010) Structure modeling of novel DNA glycosylase enzyme from oral pathogen *Streptococcus sanguinis*. Bioinformation 5(3):136–140
36. Srinivasan K, Stalin T, Sivakumar K (2012) Spectral and electrochemical study of host-guest inclusion complex between 2,4-dinitrophenol and β-cyclodextrin. Spectrochim Acta A Mol Biomol Spectrosc 94:89–100
37. Subramaniam S, Mohmmed A, Gupta D (2009) Molecular modeling studies of the interaction between Plasmodium falciparum HslU and HslV subunits. J Biomol Struct Dyn 26 (4):473–479
38. Verma S, Singh A, Mishra A (2012) Dual inhibition of chaperoning process by taxifolin: molecular dynamics simulation study. J Mol Graph Model 37:27–38
39. Verma S, Singh A, Mishra A (2012) The effect of fulvic acid on pre- and postaggregation state of Aβ(17–42): molecular dynamics simulation studies. Biochim Biophys Acta PMID:22940640
40. Venugopal S, Mohan R (2012) In silico docking studies of staphylococcus aureus virulent proteins with antimicrobial peptides. Int J Pharm Res Dev 3(12):79–86
41. Gupta S, Misra G, Pant MC, Seth PK (2011) Prediction of a new surface binding pocket and evaluation of inhibitors against huntingtin interacting protein 14: an insight using docking studies. J Mol Model 17(12):3047–3056
42. Gupta S, Misra G, Pant MC, Seth PK (2012) Targeting the epidermal growth factor receptor: exploring the potential of novel inhibitor N-(3-Ethynylphenyl)-6, 7-bis (2-methoxyethoxy) quinolin-4-amine using docking and molecular dynamics simulation. Protein Pept Lett 19(9):955–968
43. Gupta S, Misra G, Pant MC, Seth PK (2012) Identification of novel potent inhibitors aginst Bcl-XL anti-apoptotic protein using docking studies. Protein Pept Lett 19(12):1302-1317